Atmos. Chem. Phys. Discuss., 8, 20687–20722, 2008
www.atmos-chem-phys-discuss.net/8/20687/2008/

Atmospheric Chemistry and Physics Discussions

This discussion paper is/has been under review for the journal *Atmospheric Chemistry and Physics (ACP)*. Please refer to the corresponding final paper in *ACP* if available.

Multi-species inversion of CH_4, CO and H_2 emissions from surface measurements

I. Pison, P. Bousquet, F. Chevallier, S. Szopa, and D. Hauglustaine

Laboratoire des Sciences du Climat et de l'Environnement, France

Received: 4 September 2008 – Accepted: 9 October 2008 – Published: 11 December 2008

Correspondence to: I. Pison (isabelle.pison@lsce.ipsl.fr)

Published by Copernicus Publications on behalf of the European Geosciences Union.

Abstract

In order to study the spatial and temporal variations of the emissions of greenhouse gases and of their precursors, we developed a data assimilation system. It is based on the atmospheric chemical transport model LMDz and on a simplified scheme for the oxidation chain of hydrocarbons, including methane, formaldehyde, carbon monoxide and molecular hydrogen together with methyl chloroform. Inversions of the emission fluxes of CO, CH_4 and H_2 and concentrations of HCHO and OH were performed for the year 2004, using surface concentration measurements as constraints. Independent data from satellite retrievals are used to evaluate the realism of the results. The total emitted mass of CO is 30% higher after the inversion and the spatial distribution of emissions of CH_4 is modified by an increase of fluxes in boreal areas. The comparison between mono- and multi-species inversions shows that the results are close at a global scale but may significantly differ at a regional scale because of the interactions between the various tracers during the inversion.

1 Introduction

The impact of human activities on climate starts with the modification of the composition of the atmosphere. The increase in the concentrations of greenhouse gases and aerosols directly influences the radiative budget of the Earth system. Moreover, the interactions between these atmospheric compounds induce many indirect effects, with either positive or negative feedbacks on the climate. For instance, the carbon monoxide molecule (CO) does not impact atmospheric radiation much, but its concentration, through competition for hydroxyl radicals ($OH^{\bullet}$), modulates that of methane (CH_4), which is the second anthropogenic greenhouse gas after carbon dioxide (CO_2). Taking these interactions into account is an essential issue for forecasting the climate, as for interpreting the variations of the atmospheric composition. For this purpose, observation and modeling are two essential and complementary tools. Since the end

ACPD

8, 20687–20722, 2008

of the 1950s, the number of in situ measurements of atmospheric compounds has been increased several fold. Structured in international networks, the stations now provide data of a very high degree of accuracy (usually less than 0.1% for methane for example (GLOBALVIEW-CH4, last visited December 2007)) but with sparse and heterogeneous spatial coverage. The observation by satellite gradually supplements this lacunar network, though with a weaker measuring accuracy (usually around 1% for methane (Frankenberg et al., 2005)). Since the end of the 1980s, the modeling of the bio-geochemical cycles has made it possible to better understand the life cycles of greenhouse gases. Further, following the example of weather forecasting, the assimilation of bio-geochemical data in chemical transport models (CTM) has allowed, during the last decade, to produce better estimates of the emissions of gases and aerosols up to the sub-continental scale (Bergamaschi et al., 2007; Bousquet et al., 2000, 2006; Pétron et al., 2004; Rayner et al., 1999). Up to now, gas emissions have been treated independently from each other: emissions of CH_4 (Bergamaschi et al., 2007; Bousquet et al., 2006), CO (Chevallier et al., 2008; Pétron et al., 2004), dihydrogen (H_2) (Price et al., 2007) and $OH^{\bullet}$ variations (Bousquet et al., 2005; Krol et al., 2003; Prinn et al., 2005) have been optimized independently from one another, or coupled only partially (Butler et al., 2005), whereas they are linked through chemical reactions and transport. In this work, we describe the first inversion system that optimizes the four main reactive species of the methane oxidation chain (CH_4, CO, formaldehyde HCHO and H_2) within one framework. $OH^{\bullet}$ concentrations are also optimized from methyl chloroform (MCF) measurements.

The variational system used for this study, based on the Bayesian theory, is described in Sect. 2: its principal components are the global circulation model LMDz (Sect. 2.2.1) associated with the simplified chemistry model SACS (Sect. 2.2.1). In this study, the emissions that are to be optimized through the inversion are CH_4, CO and H_2 fluxes at the resolution of the grid of the model (no spatial aggregation in big regions). MCF emissions are used to constrain the optimization of $OH^{\bullet}$ concentrations within the inverse system. All the prior inventories used in the model are described in Sect. 2.3.

ACPD
8, 20687–20722, 2008

The observations used as constraints are surface measurements of MCF, CH_4, CO and H_2 concentrations (Sect. 2.4). After an evaluation of the results of the forward simulation (Sect. 3.1), the results of the inversion and an estimate of error reductions are detailed in Sect. 3.2. We then compare our optimized emissions to results obtained with different methods, particularly with mono-species inversions with the same system (Sect. 3.3), and our optimized concentrations to independent satellite, ship and aircraft data (Sect. 3.4).

2 The variational inversion system

2.1 Inversion system

The system relies on Bayesian inference as described by Chevallier et al. (2005) to combine observations and model results in order to estimate sources and sinks of atmospheric compounds. In contrast to the studies carried out up to now for the estimation of gaseous emissions (such as for example Gurney et al., 2002, Peylin et al., 2005), in this study, the inversion is formulated in a variational framework. The problem to be solved is the minimization of a cost function of a state vector $\boldsymbol{x}$, in the same way as Chevallier et al. (2005). The state vector $\boldsymbol{x}$ contains the net fluxes (sources and sinks balance) for selected species (CO, CH_4, H_2) at a given space resolution (in all model's grid cells) and at a chosen time frequency (8 days), some 3-D concentrations (HCHO and OH radicals) and the initial conditions of all concentrations (see Sect. 2.2.2 for details on species). The inversion system finds the optimal $\boldsymbol{x}_a$ that fits both the observations $\boldsymbol{y}$, the error statistics of which are represented by the covariance matrix $\mathbf{R}$, and the prior fluxes $\boldsymbol{x}_b$, for which the covariance matrix $\mathbf{B}$ specify their error statistics. The cost function J to be minimized is then defined as:

$$J(\boldsymbol{x}) = (\boldsymbol{x} - \boldsymbol{x}_b)^T \mathbf{B}^{-1} (\boldsymbol{x} - \boldsymbol{x}_b) + (H(\boldsymbol{x}) - y)^T \mathbf{R}^{-1} (H(\boldsymbol{x}) - y) \quad (1)$$

ACPD
8, 20687–20722, 2008

where H is the operator representing the chemistry-transport model plus convolution operation which gives the equivalent of observations from variables $\boldsymbol{x}$. Note that following the common usage, it is assumed that the error statistics of observations and prior information are unbiased and Gaussian, which implies that $\boldsymbol{x}_a$ also has Gaussian statistics.

The inversion system is based on the one described by Chevallier et al. (2005) to estimate CO_2 emissions. For this study, a simplified version of the module of atmospheric chemistry INCA (INteraction Chemistry – Aerosols) of Institut Pierre-Simon Laplace (IPSL), called SACS (Simplified Atmospheric Chemistry System) and detailed in Sect. 2.2.2, has been coupled to the atmospheric transport model LMDz (Laboratoire de Météorologie Dynamique – Zoom, see Sect. 2.2.1). One of the advantages of the variational formulation is its larger flexibility to deal with non-linearities in the forward model, which is important for chemistry. The minimization is performed with the algorithm M1QN3 (Gilbert and Lemaréchal, 1989). The system is ready to use satellite, aircraft and mobile or fixed surface data for the inversion of the emissions of the four species on periods of several years. In this first study, surface data are used for the inversion of emissions during the year 2004 and satellite, ship and aircraft data are used for direct comparison.

2.2 Modeling tools

2.2.1 LMDz and its adjoint

The model used here is the off-line version (LMDZt) of the general circulation model of the Laboratoire de Météorologie Dynamique (LMDZ) (Sadourny and Laval, 1984; Hourdin and Armengaud, 1999). LMDZt is used here with nineteen sigma-pressure levels in the vertical (first level thickness of 150 m, resolution in the boundary layer of 300 to 500 m and ≈2 km at tropopause) and a horizontal resolution of $3.75^\circ \times 2.5^\circ$ (longitude-latitude). The air mass fluxes used off-line were pre-calculated by LMDZ on-line GCM nudged on ECMWF analysis for horizontal winds. LMDZ has been used for

ACPD
8, 20687–20722, 2008

atmospheric studies for gases (Bousquet et al., 2005, 2006; Carouge et al., 2008a,b) and aerosols (Boucher et al., 2003) and climatological studies (IPCC, 2007).

The tangent-linear and the matching adjoint codes of the transport of non-reactive gases in LMDz, including advection, convection and turbulence in the boundary layer have been developed for this work.

2.2.2 SACS

We decided to include a simplified version of the INCA chemistry model in this study, because i) of the lack of direct observations of many of the compounds used in the full INCA model, ii) of the computational burden of the inversion with a full chemistry model and iii) of the fact that it is possible to isolate a few principal reactions in the methane oxidation chain. Consequently, INCA has been used as a reference for the development of the simplified chemical scheme displayed in Fig. 1: SACS (Hauglustaine et al., 2004; Folberth et al., 2005) is a simplified forward and adjoint chemistry module for hydrocarbon and carbon monoxide degradation.

Methane is located upstream the chemical reaction chain considered here. The nature of its sources is well established (mainly anaerobic processes in the wet lands, the rice paddies, the fires, the waste disposal sites, the ruminant stomachs, the termites, the production and the consumption of gas and oil), even if their space-time variations are still poorly given at the regional scale (Bergamaschi et al., 2007; Bousquet et al., 2006). In the atmosphere, oxidation by $OH^{\bullet}$ is the main sink of CH_4 (its lifespan is then approximately 9 years IPCC, 2007). This reaction is the first in a chain of photochemical transformations which lead to formaldehyde (HCHO or CH_2O), also produced by the degradation of volatile organic compounds (VOCs) mainly in the continental boundary layer. In the atmosphere, within a few hours, HCHO is oxidized by $OH^{\bullet}$ and photolyzed to produce CO and H_2. CO is also emitted by the combustion of biomass and fossil energies. Within a few months, CO is then oxidized by $OH^{\bullet}$ in carbon dioxide (CO_2). H_2 is also directly emitted by industries and the combustion of fossil energies and taken out of the atmosphere by deposition on the land surface (probably under the action

ACPD
8, 20687–20722, 2008

of enzymes) (Hauglustaine and Ehhalt, 2002). $OH^{\bullet}$ is the essential modulator of this reaction chain but this short-lived compound is not easily measurable. Its global concentration is observed only in an indirect way: using methyl chloroform (CH_3CCl_3 or MCF) which reacts only with $OH^{\bullet}$ and sources of which are quantified with a good accuracy (Krol et al., 2003; Prinn et al., 2005; Bousquet et al., 2005). One originality of this work is to include the constraints given by MCF concentration measurements directly within the inverse system.

The intermediate reactions not represented in Fig. 1 are regarded as very fast compared to the principal reactions above.

The adequacy of SACS has been be evaluated with the full chemistry-transport model LMDz-INCA (Hauglustaine et al., 2004; Folberth et al., 2005), as illustrated in Fig. 2: the same simulation (same meteorology, same initial conditions, those of January 2004) has been performed with the full chemistry mechanism INCA and the simplified mechanism SACS. The vertical profiles of the bias and of the standard error between the two sets of concentrations have then been computed for the five SACS tracers. The biases between the fields simulated with SACS and INCA are very small, with a maximum of 0.077 ppb (0.8×10^{-10} kg kg^{-1}) for CH_2O, −5.4 ppb (-0.3×10^{-8} kg kg^{-1}) for CH_4, −0.021 ppb (-0.2×10^{-10} kg kg^{-1}) for CO, 0.43 ppb (0.3×10^{-10} kg kg^{-1}) for H_2 and 0.003 ppb (1.3×10^{-11} kg kg^{-1}) for MCF. The field standard deviation profile indicates that the variability of the whole field as computed with INCA is 1.2 (for CH_2O at the surface) to 26.4 (for H_2 at the top) times bigger than the difference between the two mechanisms as indicated by the standard deviation profile. This means that for each one of the five species, the differences between the two chemistry models are significantly smaller than the variability of the concentration field.

Note that in order to obtain initial conditions for the simulations with SACS, LMDz-INCA is used to establish fields of $OH^{\bullet}$ and VOCs that are consistent with the initial state of the inversion system. The deposition velocities for H_2, reaction constants and photolysis rates are also given to LMDz-SACS by LMDz-INCA.

ACPD
8, 20687–20722, 2008

2.3 Emission inventory

The references used for building the prior emission inventory are listed in Table 1. The EDGAR 3 (Emission Database for Global Atmospheric Research) inventory provides anthropogenic emissions for the year 1995 with a resolution of 1×1 square degree (Olivier and Berdowski, 2001). The GFED-v2 database (van der Werf et al., 2006) provides 1×1 square degree monthly emissions due to biomass burning. Emissions from road transport and shipping have been updated in the framework of the QUANTIFY2 EU project (Quantifying the Climate Impact of Global and European Transport Systems).

The errors (variances, spatial and temporal correlations) of this prior information are modeled, based on physical considerations as detailed in Chevallier et al. (2005). In this study, correlation lengths of 500 km on land and 1000 km on sea are used (land and sea are not correlated). Through time, fluxes are defined over periods of eight days.

For 2004, the total emissions are 490 Tg of methane (including soil uptake), 1059 Tg of CO, 0.013 Tg of MCF and 39.3 Tg of H_2.

2.4 Atmospheric measurements

The observations used in this study are concentration measurements performed at surface stations for MCF, CH_4, H_2 and CO by networks available on the World Data Centre for Greenhouse Gases (WDCGG) site at http://gaw.kishou.go.jp/wdcgg/. We used instantaneous measurements and data that are 24-h averages (named "event" and "daily" data in the database). Continuous measurements by the AGAGE network were averaged over 24 h and these daily means were used. We added observations available from the RAMCES (Réseau Atmosphérique de Mesure des Composés à Effet de Serre) network coordinated by LSCE.

Among all the available stations, only those with enough measurements in 2004 (i.e. more than one value per month) were selected. The location of the stations for the

ACPD
8, 20687–20722, 2008

four tracers are displayed in Fig. 3.

For methane, all measurements were adjusted on the NOAA04 scale with the factors provided by GLOBALVIEW-CH4 (last visited December 2007).

If available, the uncertainties associated with the measurements were used. Otherwise, for CO and CH_4, we used yearly means of uncertainties from GLOBALVIEW; for MCF, we used yearly or monthly uncertainties from Prinn et al. (2005) or the NOAA; and for H_2, uncertainties from CSIRO or NOAA were used. In all cases, a minimum uncertainty of ±3 ppb for CH_4, CO and H_2 and ±1.2 ppt for MCF is fixed.

For the inversion, measurements are filtered so that only one data per grid cell per dynamical time step (30 min.) is kept. Moreover, after comparison with the a priori forward simulation, measurements for which the matching simulated concentration is out of a range of 3σ were not used as constraints for the inversion. This finally leads to keep 169 to 225 constraints per month of the year 2004 for CO, 305 to 454 for CH_4, 127 to 193 for H_2 and 264 to 302 for MCF.

3 Results

3.1 A priori forward simulation

The year 2004 is simulated by the forward model. For methane, the initial conditions have been taken from the results obtained by Bousquet et al. (2006) for 2004; for H_2, initial concentrations given by INCA, which were based on an older inventory, have been scaled by a percentage derived from the available observations; for all other tracers, the initial conditions are given by a simulation by LMDz-INCA as indicated in Sect. 2.2.2.

The performance of the a priori simulation is summarized by three statistical indicators displayed in Table 2: the bias, the standard deviation and the correlation between simulated concentrations and measurements at the stations. The weak correlation for H_2 is explained by a poor reproduction of the seasonal cycle that may be corrected by

ACPD
8, 20687–20722, 2008

the inversion of emissions.

Table 3 shows the balance between sources (emissions and chemical production) and sinks (chemical loss and deposition): it verifies that CO and CH_4 do not accumulate in the atmosphere but about 16.7 Mt of H_2 accumulate during the year. This unrealistic accumulation is partly due to a known underestimation of the deposition velocities (Hauglustaine and Ehhalt, 2002), particularly at high latitudes. A test with deposition velocities increased by 30% North of 60°of latitude shows that the accumulation of H_2 is only reduced to 15.4 Mt. Nevertheless, since no further information on deposition velocities was available at the time of this study, we chose to keep the field provided by LMDZ-INCA and test the ability of the inverse system to deal with this problem.

Note that MCF emissions are very small since early 2005, after years of large industrial use. The accumulated molecules are still being taken out of the atmosphere by chemical reaction with OH radicals. These conditions give a lifetime of about 2.6 months for CO. The values of lifetimes for CH_4, MCF and H_2 are not relevant since the forward model is not completely at equilibrium after only one year of simulation.

3.2 Inversion

The emission fluxes of CO, CH_4, H_2 and MCF have been simultaneously inverted from January to December. After 20 iterations, the norm of the gradient is reduced by about 83.2%.

Concentrations

To assess the overall impact of the optimized emissions on concentrations, first-guess and analyzed scatter-plots with simulated concentrations as function of the measurements over the whole year for all stations for each species are displayed in Fig. 4. The fit between simulated and observed CH_4 concentrations, which is already quite good for the first-guess (slope=0.98), remains almost the same after inversion with

ACPD
8, 20687–20722, 2008

a slope of 0.97 for a correlation coefficient of 0.97.
For CO concentrations, the underestimation of ≈24% by the model is reduced to ≈ 6% after inversion (slopes of 0.76 and 0.94).
As shown by the shapes and correlation coefficients for H_2 scatter-plots, the inversion only partially improves the poor fit between simulation and observations: both slopes and both correlation coefficients are still less than 0.6. Indeed, this poor fit of simulated concentrations is not caused exclusively by the emission inventory (see Sect. 3.1). The inversion corrects what can be modified by changing the emissions. Given the error statistics, it cannot propose totally unrealistic fluxes that would hide the problem on the concentrations. More work is needed on the input data and on the chemistry of H_2.
The scatter-plot for MCF clearly shows that after inversion, the concentrations are better adjusted to $OH^{\bullet}$. The small groups of points that lay outside the main clouds are an artefact of a change at one station (NWR) during the year. Since initial conditions for $OH^{\bullet}$ simply come from LMDZ-INCA interactive simulation, prior MCF and $OH^{\bullet}$ are not precisely in equilibrium. The inversion of emissions, $OH^{\bullet}$ concentrations and initial conditions is able to correct this.

The same statistical indicators as for the forward simulation are computed for the optimized emissions, as displayed in Table 2. For CO and CH_4, the median biases are largely decreased (by more than 85%) and the correlations, which were already quite good are only slightly increased after the inversion (less than +5%). The median standard deviation is slightly increased for CO but significantly decreased (by 15%) for CH_4. For H_2, the median bias, which was small for the first-guess, is increased but remains below 2 ppb, i.e. less than 0.5% of the global average measured concentration; the median standard deviation is significantly decreased (by more than 13%) and the correlation, which is low and denotes a poor seasonalization (see Sect. 3.1), is increased by almost 70%.

ACPD
8, 20687–20722, 2008

Mass budgets

The balance between sources and sinks with optimized emissions is displayed in Table 3. A small accumulation of 14.0 Mt of CO (less than 1% of the emitted mass) and of 2.8 Mt of CH_4 (less than 0.6% of the total emissions) is caused by the inversion for the year 2004. H_2 still accumulates during the year after the inversion: the non-linearity of the problem explains why the inverse system cannot totally correct the already poor first-guess. Nevertheless, the accumulated mass of H_2 in 2004 is decreased by 17.3% down to 13.4 Mt, principally through the decrease of emissions by almost 8%. More work is needed so as to fully understand the behavior of H_2 in the process.

Emissions

CO: The gradient between the two hemispheres, computed from the median values at the stations in each hemisphere, is 69 ppb for the observations and only 51 ppb for the first-guess. After optimization, the North-South gradient is 70.5 ppb: the difference with the observations is reduced by almost 92%. Thus, as displayed in Fig. 5a, the spatial distribution of corrections is not homogeneous. The emitted mass is decreased in the Southern Hemisphere, in the tropical area of South-America, in Southern Africa and in Australia, whereas it is increased by more than 60% in the boreal areas of North-America and Eurasia and in the developing India and China. As a result, the total emitted mass of CO is increased by more than 30% (Table 3). The increase of 78% and 65% in East Asia and in the Indian peninsula corresponds to the already known underestimation of CO sources in the first-guess inventories in this part of the world (Pétron et al., 2004). The increase of 62% in the boreal Canada and in Alaska can also be related to the extended fires that occurred this year, as described by Pfister et al. (2005) and Turquety et al. (2007).

CH_4: Even though the total emitted mass of CH_4 is modified by only 0.2% (Table 3), the spatial distribution of the ratio between optimized and first-guess fluxes in each pixel displayed in Fig. 5d shows that the inversion redistributes the emissions to a large

ACPD
8, 20687–20722, 2008

extent. In the Northern Hemisphere, methane fluxes are increased 1.1 to 1.4 times in three areas in the Tropics (in the center of Africa and in North India and South China) whereas they are decreased 1.1 to 2.5 times at higher latitudes (in Alaska, Scandinavia and the North of Russia).

H_2: The decrease in H_2 emissions is principally located in the center of South-America and in Africa, between 0° and 20° S, as displayed in Fig. 6, with corrections to the fluxes that are quite high locally (optimized fluxes are up to 10 times smaller). Note that since we invert net fluxes and H_2 is deposited, optimized and first-guess fluxes can have opposite signs like in South America for one pixel (pink in Fig. 6).

Error reduction

The error reduction is computed by the Monte-Carlo approach of Chevallier et al. (2007). Briefly, several inversions are run with observational constraints obtained from "true" concentrations which are actually outputs of a forward simulation, perturbed by a realization of the observation error statistics **R**. For each inversion, the seed of the random distribution and therefore the set of "measurements" is different. The first-guess fluxes are generated by perturbing the "true" fluxes with a realization of the prior error statistics **B** (see Sect. 2.1). After inversion, the difference between the "true" fluxes and the analyzed fluxes is computed and compared to the difference between the "true" and the first-guess fluxes. The error reduction is computed as the ratio of the analyzed standard deviation to the first-guess standard deviation of these differences.

The results obtained with a statistical ensemble of 96 fluxes for each pixel are displayed in Fig. 5. For CO (Fig. 5e), the reduction is larger around the stations, with reductions by more than 10% around PTA (Point Arena, California) and UTA (Wendover, Utah) on the Pacific Coast of the USA, in South Africa around CPT (Cape Point), in Australia at CFA (Cape Ferguson) and reductions up to 50% in Western Europe, where stations are close and numerous. For CH_4 (Fig. 5f), error reductions by more than 1% occur only in the Northern Hemisphere: up to 10% in Western Europe and Alaska, more than 5% on the Pacific Coast of the USA. Note that these are theoretical results

ACPD
8, 20687–20722, 2008

in the case of a statistically consistent inversion system and assuming very large prior uncertainties. Therefore, the figures for the error reduction are optimistic and only the relative variations are meaningful.

3.3 Sensitivity to multi-species inversion

In order to assess the advantage of running a multi-species inversion instead of a mono-species one as has been the case up to now, two mono-species inversions are run. In these inversions, only the emission fluxes of either CO or CH_4 are optimized (the state vector also includes initial conditions for concentrations of the same five species as for the inversion of all fluxes).

After the mono-species inversion, CO emissions are increased by 34.9% instead of 33.5% for the multi-species case, the chemical loss of CO is increased by 15% instead of 12.9% and the chemical production of CO is only changed by 0.03% (instead of 2.7%) together with the chemical loss of CH_4 which is increased by 0.06%. All the other balances are left unchanged as compared to the prior. The results obtained after the mono-species inversion are close to the results obtained for CO in the multi-species system. But the differences are that i) the median bias at the stations is −1.0 ppb after the mono-species inversion versus −0.6 ppb after the multi-species inversion and ii) the variations in percents between optimized and a priori fluxes per region are significantly different in some regions as compared to the multi-species results: +23 points in North America boreal, +6 points in USA, +6 points in Europe, +33 points in Eurasia boreal, −6 points in the Indian peninsula.

After the mono-species inversion, CH_4 emissions are increased by 3.4% to 506.9 Mt versus +0.2% for the multi-species case and the chemical production of CO is increased by 0.07%. All the other balances are left unchanged as compared to the prior. The median bias after the mono-species inversion is −0.5 ppb versus −0.1 ppb for the multi-species inversion. The difference between optimized fluxes obtained with the mono- and multi-species inversions are displayed in Fig. 7 at a pixel scale: the mono-species analyzed fluxes are higher by up to 50% than the multi-species analyzed

ACPD
8, 20687–20722, 2008

fluxes. The increase from the prior fluxes in the three tropical areas (center of Africa, North India and South China) are higher by up to 11% than with the multi-species inversion (Fig. 5d) whereas the decrease at higher latitudes (Alaska, Scandinavia, North Russia) is lower by up to 30%. These results can be explained by the fact that OH concentrations are not modified by the mono-species inversion whereas the multi-species inversion lowered them globally. Therefore, to fit the same constraints in CH_4 concentrations with higher OH concentrations i.e. with a higher chemical loss of CH_4, the mono-species inversion only has the possibility of increasing the emission fluxes.

The results obtained with the multi-species system are not globally different from the results of a mono-species inversion. The multi-species approach takes into account the complexity of the interactions between species so that consistent results are obtained in one inversion for a number of tracers. At a regional scale, the results may show significant differences as compared to the mono-species inversions: coupling CO with other species significantly changes the regional distribution of analyzed CO emissions.

3.4 Comparison with other data

We compare the results of our multi-species inversion to results obtained in another study inverting one of the species of interest and to observation data (satellite, aircraft and ship data) that have not been used in our inversions.

Other inversion system: For CH_4, Bousquet et al. (2006) computed a range of emissions for 2004, compared in Table 4 to our results in seven areas. For four regions (North and South Americas, Europe, South Asia), our estimate is within this range; for two other regions (Boreal Eurasia and India+China) our emissions are above the maximum by 8.4 and 3.1%; in Africa, our result is under the minimum by 13%. Comparing the results for the tropical regions indicates a shift of emissions from South America and Africa for the study of Bousquet et al. (2005) to India+China in our study. This difference in attributing methane emissions in the Tropics may be due to the cumulative effects of aggregation errors for the study of Bousquet et al. (2005) and to the small number of available stations in this area for both studies. Our CH_4 optimized emissions

seem to be statistically consistent with the results of a completely different system.

Mobile surface and aircraft CH_4 measurements: For the year 2004, 456 mobile surface observations of CH_4 concentrations are available through the Pacific Ocean, Atlantic Ocean and Western Pacific Cruises (POC, AOC, WPC), ships in the North Atlantic (CVS) and in the Indian Ocean (MDF, Marion Dufresne ship) and 202 tri-dimensional observations are given by aircraft measurements made in Hungary (HNG) and in France (ORL) (locations displayed in Fig. 8). These data were compared to simulated concentrations before and after inversion through scatter-plots (not shown): the results of the regressions of simulated concentrations as functions of observations are displayed in Table 5.

The fit between simulation and mobile surface data (2-D-data), which is already quite good as a first-guess, is slightly better after inversion: the slope is increased from 0.97 to 0.98 for the same correlation coefficient. Since these measurements are made in the oceans, far from the sources, this shows that simulated background concentrations are improved by the inversion.

The aircraft data in the boundary layer (113 measurements) show an overestimation by the model before inversion (slope = 1.14) which is changed into an underestimation of the same intensity after the optimization of emissions. The vertical profiles of root mean square (RMS) and standard deviation between measurements and the first-guess or analyzed simulated CH_4 concentrations are displayed in Fig. 9. They show that the inversion has a positive impact on the RMS and on the standard deviation: the RMS are reduced by 9 to 16.5% at HNG and 1 to 31% at ORL and the standard deviation are reduced by 7.5 to 16.5% at HNG and 1.5 to 32% at ORL. At ORL in particular, the vertical profiles show that the improvement in the RMS is due to a decrease in the standard deviation and not in the bias.

Satellite data: MOPITT CO measurements are available for 2004, we use here retrievals at 700 hPa of concentration product (level 2 version 5) with individual averaging kernels (Deeter et al., 2003) as described by Chevallier et al. (2008). Since there is a strong gradient between the two hemispheres, the data are compared to simulated

ACPD
8, 20687–20722, 2008

concentrations before and after inversion through scatter-plots for the Northern and the Southern Hemispheres separately: the results of the regressions of simulated concentrations as functions of observations are displayed in Table 5. The inversion increases by 24 and 12% the slopes in the Northern and Southern Hemispheres respectively. Nevertheless, the comparison with MOPITT shows an underestimation by ≈ 22% of analyzed CO concentrations in the Northern Hemisphere that could be due to difficulties to reproduce the high emissions due to the fires that occurred in 2004 in Alaska and Canada boreal areas (see paragraph "Emissions" in Sect. 3.2).

4 Conclusions

We have developed a variational system based on the LMDz transport model and on a simplified chemistry system representing the oxidation chain of methane, to perform multi-species inversions of CH_4, CO and H_2 surface emissions at model resolution and for the year 2004. $OH^{\bullet}$ concentrations are optimized simultaneously, as constrained by methyl-chloroform atmospheric observations.

Results show significant modifications in the total emitted masses and in the spatial distribution of emissions. For CO, the total emitted mass is increased by 30%. A large increase of more than 65% in the regions of East Asia and the Indian peninsula corrects for the known underestimation of CO emissions in these rapidly industrializing areas. A particular feature of the year 2004 is captured in boreal North America: the increase of more than 60% of CO emissions in Alaska and Canada may be related to the intense fires that occurred this year. For almost the same total emissions, the spatial distribution of CH_4 fluxes is significantly modified with increased fluxes in the Tropics (+10 to +40% in Africa, India and China) and decreased fluxes in boreal areas (−10 to −60% in Alaska, Scandinavia and Russia). Estimated error reductions for analyzed emissions are larger in Western Europe (50% for CO and 10% for CH_4) because of the higher density of the measurement networks in this area.

Even though the global balances obtained with the multi-species system are not

ACPD
8, 20687–20722, 2008

very different from the results of a mono-species inversion at the global scale, regional differences are significant, particularly for CH_4 (in North America, Europe, boreal Eurasia and India). In practice, the analyzed fluxes of all the tracers are obtained in one consistent inversion.

The comparison of our analyzed fluxes with the results obtained by another inversion system shows that they lay in the same range. The comparison of our analyzed CH_4 concentrations with independent measurements by mobile surface stations and aircraft shows a better fit for the background conditions (on the oceans) and a significant improvement in the vertical profiles in the boundary layer and in the free troposphere (RMS and standard deviation). The comparison of CO concentrations to independent satellite data shows that the fit between simulation and measures is significantly better in both hemispheres after the inversion.

The next step is now to integrate the satellite data used here for validation, as new constraints for a multi-species inversion using SCIAMACHY methane columns, MOPITT CO columns and ultimately, surface data simultaneously.

Acknowledgements. The authors contacted all data PIs and thank E. Brunke (SAWS), B. Buchmann (EMPA), D. Cunnold (AGAGE), E. Dlugokencky (NOAA), G. Dutton (NOAA), J. W. Elkins (NOAA), A. Gomez (NIWA), P. Krummel (CSIRO), R. Langenfelds (CSIRO), K. Masarie (NOAA), S. A. Montzka (NOAA), P. C. Novelli (NOAA) , T. Seitz (EMPA), K. Tsuboi (JMA), K. Uhse, L. Ries and F. Meinhardt (UBA) and D. Worthy (Environment Canada) for providing the observation data through the World Data Centre for Greenhouse Gases. We thank M. Schmidt for providing LSCE measurements. MOPITT data were obtained from the Atmospheric Science Data Center (NASA Langley Research Center) and prepared for our use by A. Fortems (LSCE). The authors also wish to thank the computing support team of LSCE. This work was done in the framework of the HYMN Project funded by the EU 6th Framework Programme (GOCE).

CENTRE NATIONAL DE LA RECHERCHE SCIENTIFIQUE INSU

The publication of this article is financed by CNRS-INSU.

References

Bergamaschi, P., Frankenberg, F., Meirink, J. F., Krol, M., Dentener, F., Wagner, T., Platt, U., Kaplan, J. O., Körner, S., Heimann, M., Dlugokencky, E. J., and Goede, A.: Satellite chartography of atmospheric methane from SCIAMACHY on board ENVISAT: 2. Evaluation based on inverse model simulations, J. Geophys. Res., 112, D02304, doi:10.1029/2006JD007268, 2007. 20689, 20692

Boucher, O., Moulin, C., Belviso, S., Aumont, O., Bopp, L., Cosme, E., von Kuhlmann, R., Lawrence, M. G., Pham, M., Reddy, M. S., Sciare, J., and Venkataraman, C.: DMS atmospheric concentrations and sulphate aerosol indirect radiative forcing: a sensitivity study to the DMS source representation and oxidation, Atmos. Chem. Phys., 3, 49–65, 2003, http://www.atmos-chem-phys.net/3/49/2003/. 20692

Bousquet, P., Peylin, P., Ciais, P., Le Quere, C., Friedlingstein, P., and Tans, P.: Regional changes in carbon dioxide fluxes of land and ocean since 1980, Science, 290, 1342–1345, 2000. 20689

Bousquet, P., Hauglustaine, D. A., Peylin, P., Carouge, C., and Ciais, P.: Two decades of OH variability as inferred by an inversion of atmospheric transport and chemistry of methyl chloroform, Atmos. Chem. Phys., 5, 2635–2656, 2005, http://www.atmos-chem-phys.net/5/2635/2005/. 20689, 20692, 20693, 20701, 20712

Bousquet, P., Ciais, P., Miller, J. B., Dlugokencky, E. J., Hauglustaine, D. A., Prigent, C., Van der Werf, G. R., Peylin, P., Brunke, E. G., Carouge, C., Langenfelds, R. L., Lathiere, J., Papa, F., Ramonet, M., Schmidt, M., Steele, L. P., Tyler, S. C., and White, J.: Contribution of anthropogenic and natural sources to atmospheric methane variability, Nature, 443, 439–443, doi:10.1038/nature05132, 2006. 20689, 20692, 20695, 20701

Butler, T. M., Rayner, P. J., Simmonds, I., and Lawrence, M. G.: Simultaneous mass balance inverse modeling of methane and carbon monoxide, J. Geophys. Res., 110, D21310, doi:10.1029/2005JD006071, 2005. 20689

Carouge, C., Bousquet, P., Peylin, P., Rayner, P. J., and Ciais, P.: What can we learn from European continuous atmospheric CO_2 measurements to quantify regional fluxes – Part 1: Potential of the network, Atmos. Chem. Phys. Discuss., 8, 18 591–18 620, 2008a, http://www.atmos-chem-phys-discuss.net/8/18591/2008/. 20692

Carouge, C., Peylin, P., Rayner, P. J., Bousquet, P., Chevallier, F., and Ciais, P.: What can we learn from European continuous atmospheric CO_2 measurements to quantify regional

fluxes – Part 2: Sensitivity of flux accuracy to inverse setup, Atmos. Chem. Phys. Discuss., 8, 18 621–18 649, 2008b, http://www.atmos-chem-phys-discuss.net/8/18621/2008/. 20692

Chevallier, F., Fisher, M., Peylin, P., Serrar, S., Bousquet, P., Bréon, F.-M., Chédin, A., and Ciais, P.: Inferring CO_2 sources and sinks from satellite observations: method and application to TOVS data, J. Geophys. Res., 110, D24309, doi:10.1029/2005JD006390, 2005. 20690, 20691, 20694

Chevallier, F., Bréon, F.-M., and Rayner, P.: The contribution of the Orbiting Carbon Observatory to the estimation of CO_2 sources and sinks: Theoretical study in a variational data assimilation framework, J. Geophys. Res., 112, D09307, doi:10.1029/2006JD007375, 2007. 20699

Chevallier, F., Fortems, A., Bousquet, P., Pison, I., Szopa, S., Devaux, M., and Hauglustaine, D. A.: African CO emissions between years 2000 and 2006 as estimated from MOPITT observations, Biogeosciences Discuss., 5, 3845–3868, 2008, http://www.biogeosciences-discuss.net/5/3845/2008/. 20689, 20702

Deeter, M., Emmons, L., Francis, G., Edwards, D., Gille, J., Warner, J., Khattatov, B., Ziskin, D., Lamarque, J.-F., Ho, S.-P., Yudin, V., Attié, J.-L., Packman, D., Chen, J., Mao, D., and Drummond, J.: Operational carbon monoxide retrieval algorithm and selected results for the MOPITT instrument, J. Geophys. Res., 108, 4399, doi:10.1029/2002JD003186, 2003. 20702

Folberth, G., Hauglustaine, D., Ciais, P., and Lathière, J.: On the role of atmospheric chemistry in the global CO_2 budget, Geophys. Res. Lett., 32, L08801, doi:10.1029/2004GL021812, 2005. 20692, 20693

Frankenberg, C., Meirink, J., van Weele, M., Platt, U., and Wagner, T.: Assessing methane emissions from global space-borne observations, Science, 308, 1010–1014, doi:10.1126/science.1106644, 2005. 20689

Fung, I., John, J., Lerner, J., Matthews, E., Prather, M., Steele, L., and Fraser, P.: Three-dimensional model synthesis of the global methane cycle, J. Geophys. Res., 96, 13 033–13 065, 1991. 20709

Gilbert, J.-C. and Lemaréchal, C.: Some numerical experiments with variable-storage quasi-Newton algorithms, Mathematical programming, 45, 407–435, 1989. 20691

GLOBALVIEW-CH4: http://www.esrl.noaa.gov/gmd/ccgg/globalview/ch4/ch4_intro.html, last access: Dec 2007. 20689, 20695

Gurney, K., Law, R., Denning, A., Rayner, P., Baker, D., Bousquet, P., Bruhwiler, L., Chen, Y.,

Ciais, P., Fan, S., Fung, I., Gloor, M., Heimann, M., Higuchi, K., John, J., Maki, T., Maksyutov, S., Masarie, K., Peylin, P., Prather, M., Pak, B., Randerson, J., Sarmiento, J., Taguchi, S., Takahashi, T., and Yuen, C.: Towards robust regional estimates of CO_2 sources and sinks using atmospheric transport models, Nature, 415, 626–630, 2002. 20690

Hauglustaine, D. and Ehhalt, D.: A three-dimensional model of molecular hydrogen in the troposphere, J. Geophys. Res., 107, 4330, doi:10.1029/2001JD001156, 2002. 20693, 20696, 20709

Hauglustaine, D., Hourdin, F., Jourdain, L., Filiberti, M., Walters, S., Lamarque, J., and Holland, E.: Interactive chemistry in the Laboratoire de Météorologie Dynamique general circulation model: Description and background tropospheric chemistry evaluation, J. Geophys. Res., 109, D04314, doi:10.1029/2003JD003957, 2004. 20692, 20693

Hourdin, F. and Armengaud, A.: The use of finite-volume methods for atmospheric advection of trace species. Part I: Test of various formulations in a general circulation model, Mon. Weather Rev., 127, 822–837, 1999. 20691

IPCC: Climate change 2007 – Synthesis Report, Cambridge University Press, 2007. 20692

Krol, M., Lelieveld, J., Oram, D., Sturrock, G., Penkett, S., Brenninkmeijer, C., Gros, V., Williams, J., and Scheeren, H.: Continuing emissions of methyl chloroform from Europe, Nature, 421, 131–135, doi:10.1038/nature01311, 2003. 20689, 20693

Lathière, J., Hauglustaine, D., de Noblet-Ducoudré, N., Krinner, G., and Folberth, G. A.: Past and future changes in biogenic volatile organic compound emissions simulated with a global dynamic vegetation model, Geophys. Res. Lett., 32, L20818, doi:10.1029/2005GL024164, 2005. 20709

Olivier, J. G. J. and Berdowski, J. J. M.: The Climate System, chap. Global emissions sources and sinks, edited by: Berdowski, J., Guichert, R., Heij, B., A. A. Balkema/Swets & Zeitlinger, 33–37, 2001. 20694

Pétron, G., Granier, C., Khattatov, B., Yudin, V., Lamarque, J., Emmons, L., Gille, J., and Edwards, D.: Monthly CO surface sources inventory based on the 2000-2001 MOPITT satellite data, Geophys. Res. Lett., 31, L21107.1–L21107.5, doi:10.1029/2004GL020560, 2004. 20689, 20698

Peylin, P., Rayner, P. J., Bousquet, P., Carouge, C., Hourdin, F., Heinrich, P., Ciais, P., and AEROCARB contributors: Daily CO_2 flux estimates over Europe from continuous atmospheric measurements: 1, inverse methodology, Atmos. Chem. Phys., 5, 3173–3186, 2005, http://www.atmos-chem-phys.net/5/3173/2005/. 20690

Pfister, G., Hess, P., Emmons, L., Lamarque, J.-F., Wiedinmyer, C., Edwards, D., Pétron, G., Gille, J., and Sachse, G.: Quantifying CO emissions from the 2004 Alaskan wildfires using MOPITT CO data, Geophys. Res. Lett., 32, L11809, doi:10.1029/2005GL022995, 2005. 20698

Price, H., Jaeglé, L., Rice, A., Quay, P., Novelli, P. C., and Gammon, R.: Global budget of molecular hydrogen and its deuterium content: Constraints from ground station, cruise, and aircraft observations, J. Geophys. Res., 112, D22108, doi:10.1029/2006JD008152, 2007. 20689

Prinn, R., Huang, J., Weiss, R., Cunnold, D., Fraser, P., Simmonds, P., McCulloch, A., Harth, C., Reimann, S., Salameh, P., O'Doherty, S., Wang, R., Porter, L., Miller, B., and Krummel, P.: Evidence for variability of atmospheric hydroxyl radicals over the past quarter century, Geophys. Res. Lett., 32, L07809, doi:10.1029/2004GL022228, 2005. 20689, 20693, 20695

Rayner, P. J., Enting, I. G., Francey, R. J., and Langenfelds, R.: Reconstructing the recent carbon cycle from atmospheric CO_2,$\delta^{13}C$ and O_2/N_2 observations, Tellus B, 51, 213–232, 1999. 20689

Sadourny, R. and Laval, K.: New Perspectives in Climate Modeling, chap. January and July performance of the LMD general circulation model, edited by: Bergerand, A. L. and Nicolis, C., Amsterdam, Elsevier Press edn., 173–197, 1984. 20691

Turquety, S., Logan, J. A., Jacob, D. J., Hudman, R. C., Leung, F. Y., Heald, C. L., Yantosca, R. M., Wu, S., Emmons, L. K., Edwards, D. P., and Sachse, G. W.: Inventory of boreal fire emissions for North America in 2004: Importance of peat burning and pyroconvective injection, J. Geophys. Res., 112, D12S03, doi:10.1029/2006JD007281, 2007. 20698

van der Werf, G. R., Randerson, J. T., Giglio, L., Collatz, G. J., Kasibhatla, P. S., and Arellano Jr., A. F.: Interannual variability in global biomass burning emissions from 1997 to 2004, Atmos. Chem. Phys., 6, 3423–3441, 2006, http://www.atmos-chem-phys.net/6/3423/2006/. 20694, 20709

Table 1. References for the prior emission inventory. VOCs=Volatile Organic Compounds, MCF=methyl chloroform.

Species	Anthropogenic emissions	Biogenic emissions
VOCs	EDGAR 3	ORCHIDEE vegetation model (Lathière et al., 2005)
MCF	EDGAR 3	–
CO	EDGAR 3	biomass burning: GFED-v2 road transport and shipping: QUANTIFY2 EU
CH_4	EDGAR 3	wetlands: Fung et al. (1991) biomass burning: van der Werf et al. (2006)
H_2	EDGAR 3	Hauglustaine and Ehhalt (2002)

ACPD
8, 20687–20722, 2008

Table 2. Median values over all the stations for bias, standard deviation and correlation between measured and simulated concentrations in 2004: before inversion, **after inversion** and *difference in %* of the prior value between the a priori and a posteriori simulations.

Species	bias (ppb)		standard deviation (ppb)		correlation	
	prior	analysis	prior	analysis	prior	analysis
MCF	$9.8.10^{-4}$	**$-4.1.10^{-4}$**	$4.6.10^{-4}$	**$4.2.10^{-4}$**	0.96	**0.96**
CO	10.7	**–0.6**	9.1	**9.6**	0.86	**0.9**
	–94%		*+5.5%*		*+4.6%*	
CH_4	−0.8	**–0.1**	11.3	**9.6**	0.81	**0.82**
	–87%		*–15%*		*+1.2%*	
H_2	−0.9	**1.8**	15.9	**13.8**	0.22	**0.37**
	+100%		*–13.2%*		*+68.2%*	

ACPD
8, 20687–20722, 2008

Table 3. Mass balances in Mt for the year 2004: before inversion, **after inversion** and *difference in %* of the prior value between before and after inversion.

Species	emissions	chemical production	chemical loss	deposition
MCF	0.013106 **0.013106**	–	0.081625 **0.084252**	–
CO	1058.6 **1413.**	1212.2 **1179.3**	2284. **2578.3**	–
	+33.5%	*–2.7%*	*+12.9%*	
CH_4	490.4 **491.5**	–	504. **488.7**	–
	+0.2%		*–3%*	
H_2	39.3 **36.2**	39.3 **38.6**	18.6 **17.9**	43.8 **43.5**
	–7.9%	*–1.8%*	*–3.8%*	*–0.7%*

ACPD
8, 20687–20722, 2008

Table 4. Total emitted CH_4 masses (Mt) during 2004 for Bousquet et al. (2006) and this study.

Area	Bousquet et al. (2005) prior	*optimization range*	this study *optimized*	prior
North America	104.4	*59.4–77.5*	*67.7*	67.
South America	141.3	*67.–94.8*	*67.1*	71.8
Europe	91.9	*51.9–64.6*	*56.3*	58.1
Africa	93.	*74.8–95.*	*64.1*	53.8
Boreal Eurasia	58.8	*22.3–28.1*	*28.5*	32.3
India+China	150.1	*113.9–149.6*	*162.6*	152.4
Australia+Indonesia	68.4	*38.5–54.9*	*44.7*	45.1

ACPD
8, 20687–20722, 2008

Table 5. Linear regression coefficients for simulated concentrations as a function of observation data with slope *a* and correlation coefficient *r*. BL=Boundary Layer, up to ≈1100 m in the model. NH=Northern Hemisphere, SH=Southern Hemisphere.

Species	Type of measurements	Coefficients	First-guess	Analysis
CH_4	2-D-data	*a*	0.97	0.98
		r	0.96	0.96
	3-D-data (BL)	*a*	1.14	0.86
		r	0.73	0.7
CO	MOPITT NH	*a*	0.63	0.78
		r	0.57	0.58
	MOPITT SH	*a*	0.85	0.95
		r	0.77	0.78

ACPD
8, 20687–20722, 2008

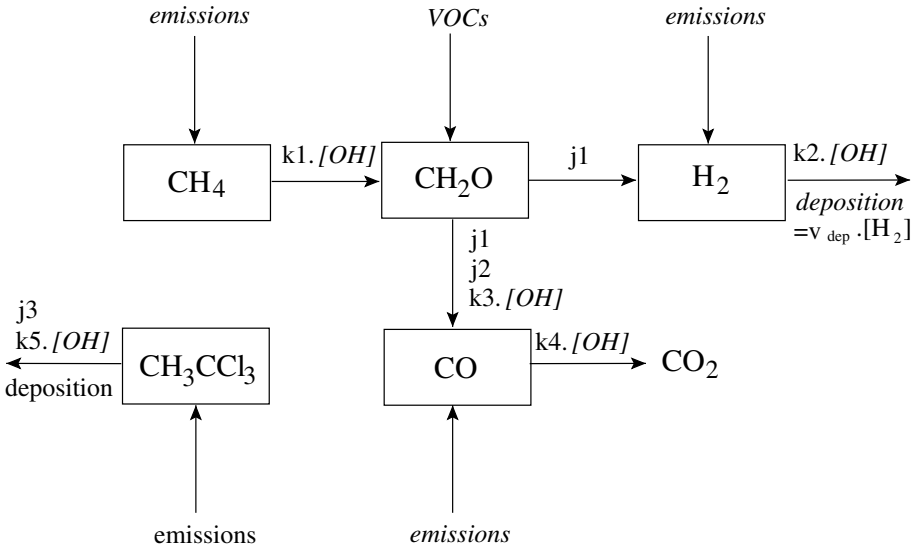

Fig. 1. Schematic of the simplified chemistry mechanism SACS: j1-3 and k1-5 are the constants of the reactions or of ensembles of reactions. [OH] and the variables indicated in italics are directly optimized by the data assimilation system.

ACPD
8, 20687–20722, 2008

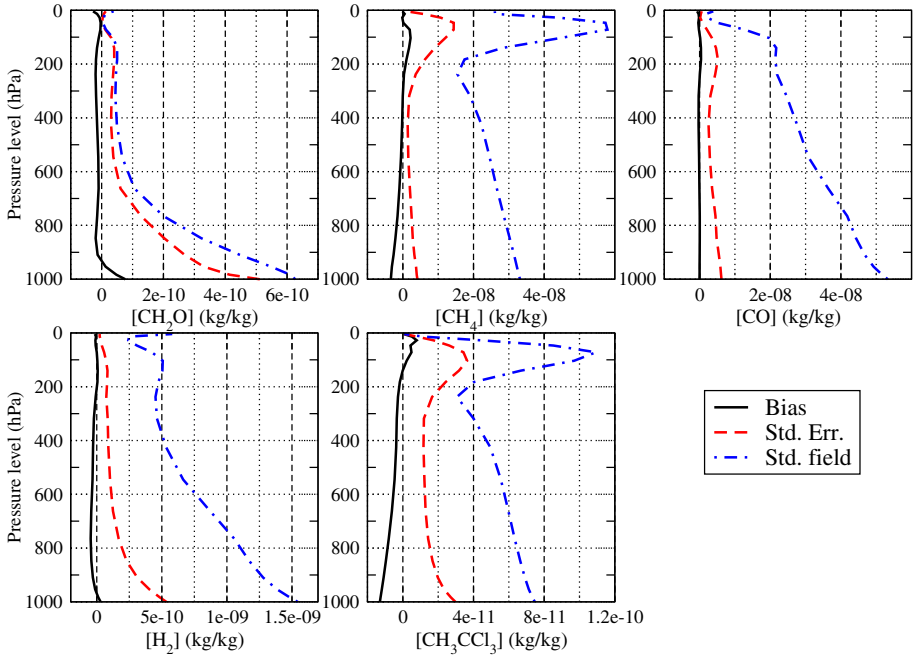

Fig. 2. Vertical profiles of bias and standard deviation (Std. Err.) of the differences between concentrations ($kg\,kg^{-1}$) of formaldehyde (CH_2O), methane (CH_4), carbon monoxide (CO), di-hydrogen (H_2) and methyl chloroform (CH_3CCl_3=MCF) obtained with the simplified chemistry mechanism SACS and the full chemistry mechanism INCA: example of January 2004. The field standard deviation (Std. field) profile corresponds to the field computed with INCA.

ACPD
8, 20687–20722, 2008

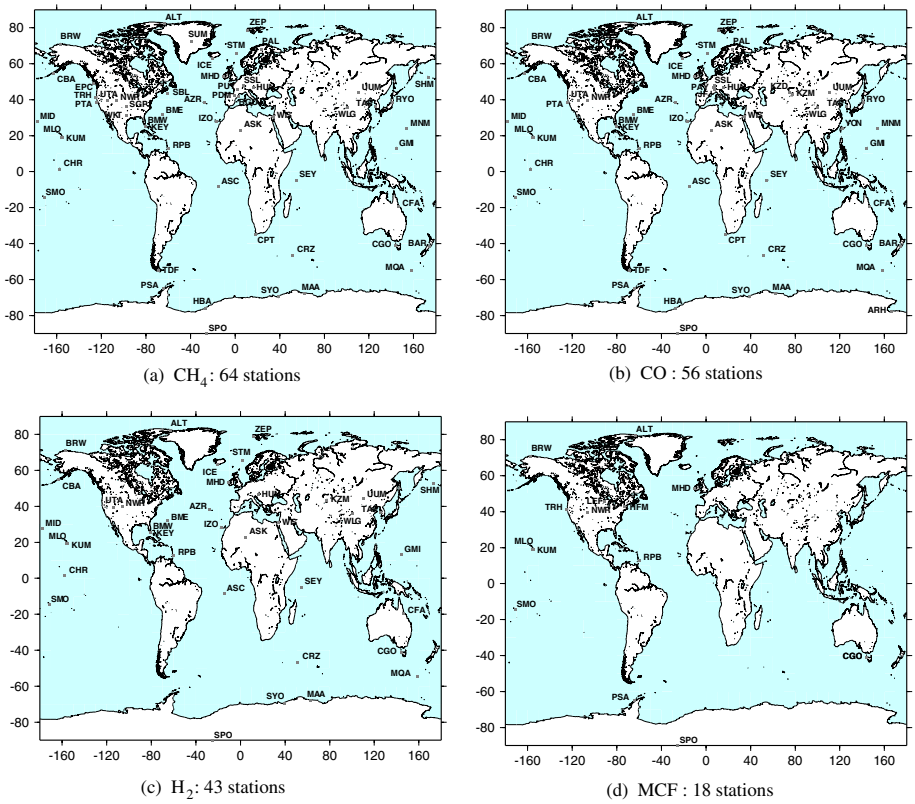

Fig. 3. Measurement surface stations for methane, carbon monoxide, dihydrogen and MCF used in our study over the year 2004.

ACPD
8, 20687–20722, 2008

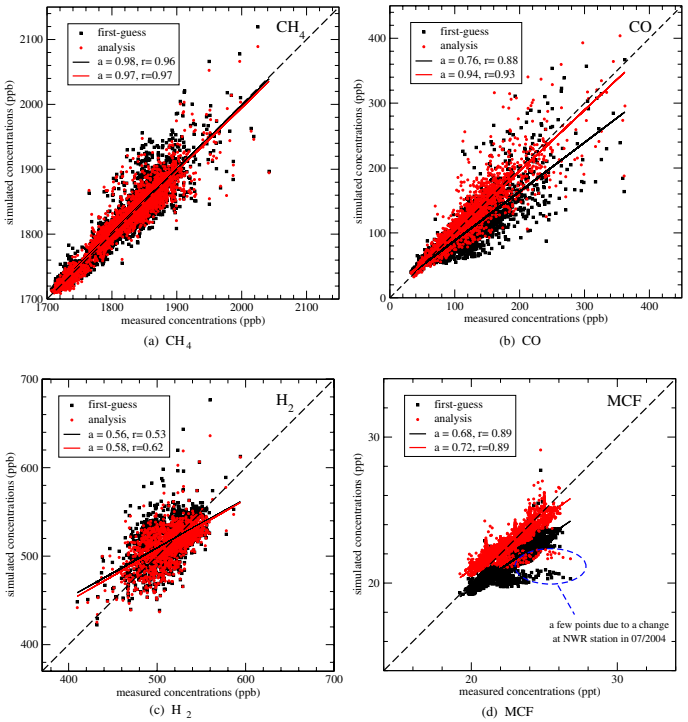

Fig. 4. Simulated first-guess and analyzed concentrations as functions of measurements at all stations over the whole year 2004 for methane, carbon monoxide, dihydrogen and MCF. Linear regressions [mod]=*a*.[obs]+*b* with correlation coefficient *r*.

ACPD
8, 20687–20722, 2008

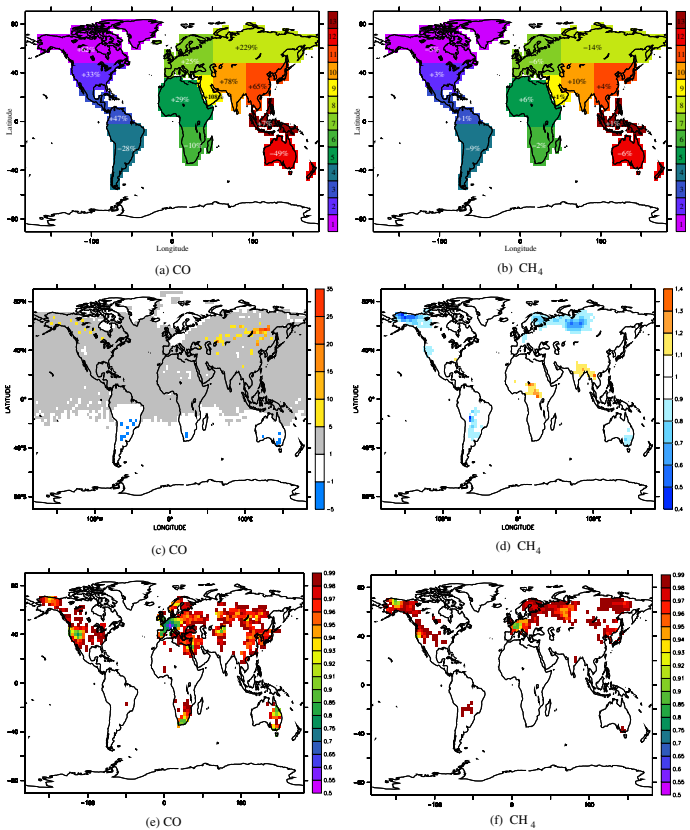

Fig. 5. **(a–b)** Difference in % between optimized and a priori emission fluxes per region for 2004. 1=North America boreal, 2=USA, 3=America tropical, 4=South America temperate, 5=Northern Africa, 6=Southern Africa, 7=Europe, 8=Eurasia boreal, 9=Middle East, 10=Indian peninsula, 11=East Asia, 12=Australia, 13=Indonesia. **(c–d)** Ratio between optimized and a priori emission fluxes per pixel for 2004. **(e–f)** Error reduction for CO and CH_4 fluxes computed from statistics of 96 realizations per pixel.

ACPD
8, 20687–20722, 2008

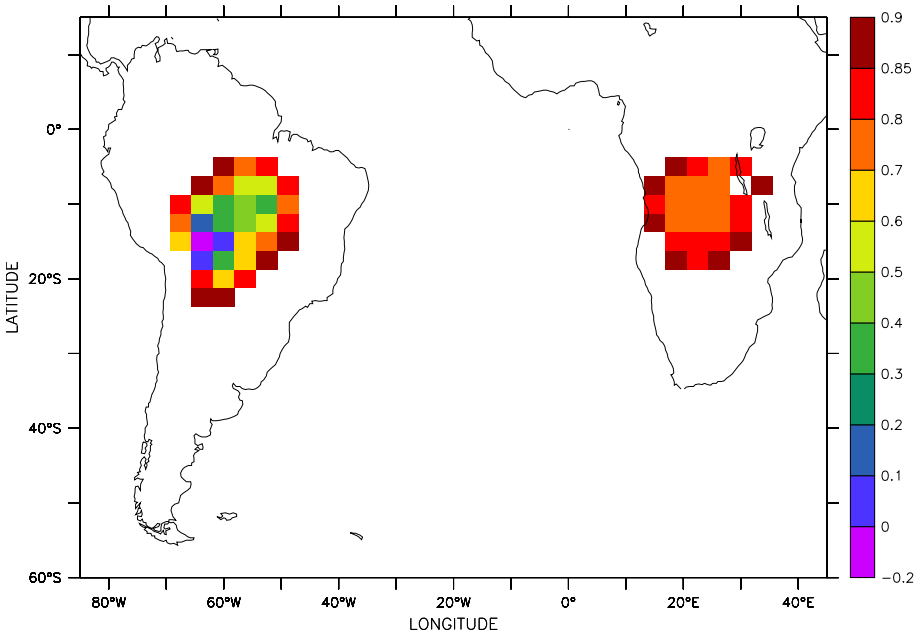

Fig. 6. Ratio between optimized and a priori H_2 emission fluxes per pixel for 2004, focus on South America and Africa.

ACPD
8, 20687–20722, 2008

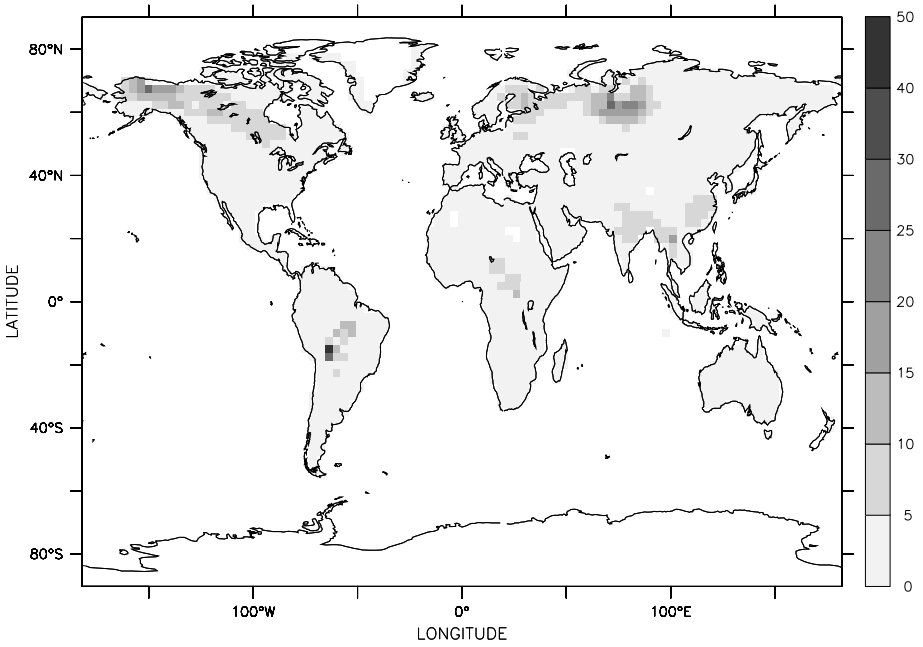

Fig. 7. Difference between mono- and multi-species optimized CH_4 emission fluxes (in % of the multi-species optimized fluxes) per pixel for 2004.

ACPD
8, 20687–20722, 2008

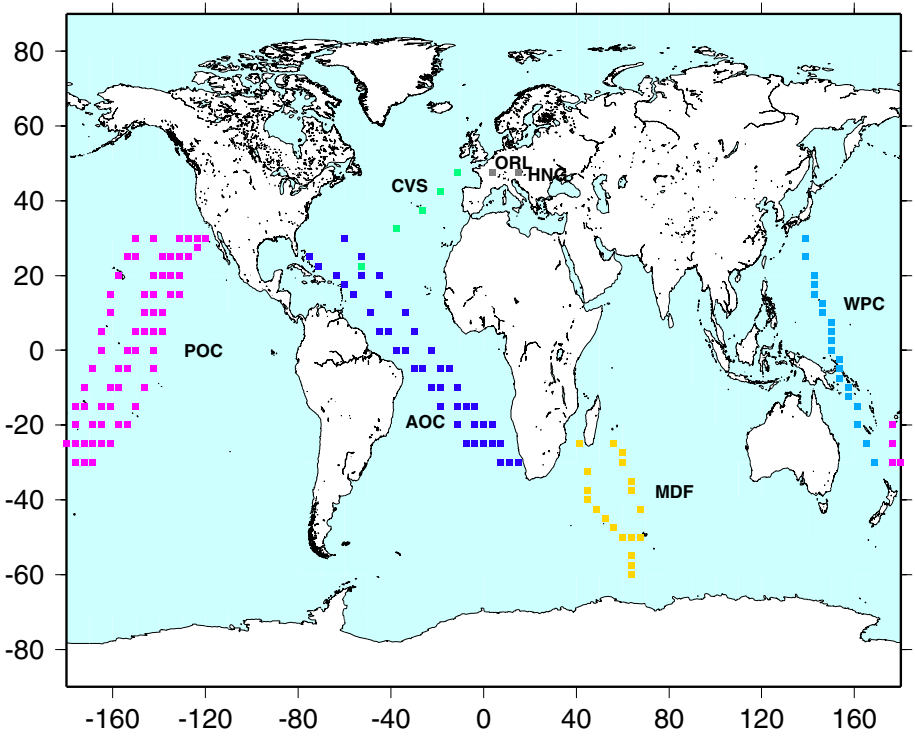

Fig. 8. Locations of the 2-D- and 3-D-mobile measurements of CH_4 concentrations for 2004.

ACPD
8, 20687–20722, 2008

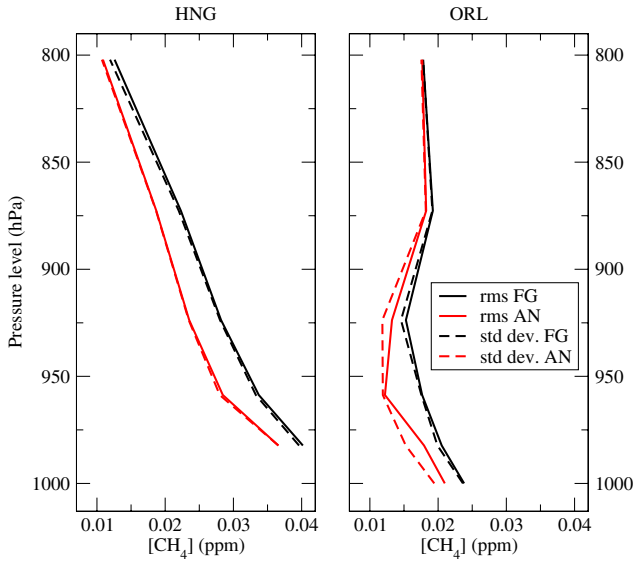

Fig. 9. Vertical profiles of root mean square (rms) and standard deviation (std dev.) between measured and first-guess (FG) or analyzed (AN) CH_4 concentrations (ppb) at ORL and HNG locations in 2004.

ACPD
8, 20687–20722, 2008